The current issue and full text archive of this journal is available at
www.emeraldinsight.com/1757-9864.htm

All-atom molecular-level computational analyses of polyurea/fused-silica interfacial decohesion caused by impinging tensile stress-waves

Received 4 January 2014
Revised 3 March 2014
Accepted 24 April 2014

M. Grujicic, R. Yavari, J.S. Snipes and S. Ramaswami
Department of Mechanical Engineering, Clemson University, Clemson, South Carolina, USA, and
R.S. Barsoum
Office of Naval Research, Ships and Engineering Systems Division, Arlington, Virginia, USA

Abstract

Purpose – The purpose of this paper is to address the problems of interaction of tensile stress-waves with polyurea/fused-silica and fused-silica/polyurea interfaces, and the potential for the accompanying interfacial decohesion.

Design/methodology/approach – The problems are investigated using all-atom non-equilibrium molecular-dynamics methods and tools. Before these methods/tools are employed, previously determined material constitutive relations for polyurea and fused-silica are used, within an acoustic-impedance-matching procedure, to predict the outcome of the interactions of stress-waves with the material-interfaces in question. These predictions pertain solely to the stress-wave/interface interaction aspects resulting in the formation of transmitted and reflected stress- or release-waves, but do not contain any information regarding potential interfacial decohesion. Direct molecular-level simulations confirmed some of these predictions, but also provided direct evidence of the nature and the extent of interfacial decohesion. To properly model the initial state of interfacial cohesion and its degradation during stress-wave-loading, reactive forcefield potentials are utilized.

Findings – Direct molecular-level simulations of the polyurea/fused-silica interfacial regions prior to loading revealed local changes in the bonding structure, suggesting the formation of an interphase. This interphase was subsequently found to greatly affect the polyurea/fused-silica decohesion strength.

Originality/value – To the authors' knowledge, the present work is the first public-domain report of the use of the non-equilibrium molecular dynamics and reactive force-field potentials to study the problem of interfacial decohesion caused by the interaction of tensile waves with material interfaces.

Keywords Polyurea, Fused silica, Interfacial decohesion, Reactive forcefields

Paper type Research paper

The material presented in this paper is based on work supported by the Office of Naval Research (ONR) research contract entitled "Elastomeric Polymer-By-Design to Protect the Warfighter Against Traumatic Brain Injury by Diverting the Blast Induced Shock Waves from the Head", Contract Number 4036-CU-ONR-1125 as funded through the Pennsylvania State University, and the Army Research Office (ARO) research contract entitled "Friction Stir Welding Behavior of Selected 2000-series and 5000-series Aluminum Alloys", Contract Number W911NF-11-1-0207. The authors are indebted to Dr Ralph A. Anthenien Jr of ARO for his continuing support and interest in the present work.

International Journal of Structural Integrity
Vol. 5 No. 4, 2014
pp. 339-367

1757-9864
DOI 10.1108/IJSI-01-2014-0001

Report Documentation Page

Form Approved
OMB No. 0704-0188

1. REPORT DATE	2. REPORT TYPE	3. DATES COVERED
2014		**00-00-2014 to 00-00-2014**

4. TITLE AND SUBTITLE
All-atom Molecular-level Computational Analyses of Polyurea/fused-silica Interfacial Decohesion Caused by Impinging Tensile Stress-waves

5a. CONTRACT NUMBER
5b. GRANT NUMBER
5c. PROGRAM ELEMENT NUMBER

6. AUTHOR(S)

5d. PROJECT NUMBER
5e. TASK NUMBER
5f. WORK UNIT NUMBER

7. PERFORMING ORGANIZATION NAME(S) AND ADDRESS(ES)
Clemson University,Department of Mechanical Engineering,241 Engineering Innovation Building,Clemson,SC,29634

8. PERFORMING ORGANIZATION REPORT NUMBER

9. SPONSORING/MONITORING AGENCY NAME(S) AND ADDRESS(ES)

10. SPONSOR/MONITOR'S ACRONYM(S)
11. SPONSOR/MONITOR'S REPORT NUMBER(S)

12. DISTRIBUTION/AVAILABILITY STATEMENT
Approved for public release; distribution unlimited

13. SUPPLEMENTARY NOTES

14. ABSTRACT

Purpose ??? The purpose of this paper is to address the problems of interaction of tensile stress-waves with polyurea/fused-silica and fused-silica/polyurea interfaces, and the potential for the accompanying interfacial decohesion. Design/methodology/approach ??? The problems are investigated using all-atom non-equilibrium molecular-dynamics methods and tools. Before these methods/tools are employed, previously determined material constitutive relations for polyurea and fused-silica are used, within an acoustic-impedance-matching procedure, to predict the outcome of the interactions of stress-waves with the material-interfaces in question. These predictions pertain solely to the stress-wave/interface interaction aspects resulting in the formation of transmitted and reflected stress- or release-waves, but do not contain any information regarding potential interfacial decohesion. Direct molecular-level simulations confirmed some of these predictions, but also provided direct evidence of the nature and the extent of interfacial decohesion. To properly model the initial state of interfacial cohesion and its degradation during stress-wave-loading, reactive forcefield potentials are utilized. Findings ??? Direct molecular-level simulations of the polyurea/fused-silica interfacial regions prior to loading revealed local changes in the bonding structure, suggesting the formation of an interphase. This interphase was subsequently found to greatly affect the polyurea/fused-silica decohesion strength. Originality/value ??? To the authors??? knowledge, the present work is the first public-domain report of the use of the non-equilibrium molecular dynamics and reactive force-field potentials to study the problem of interfacial decohesion caused by the interaction of tensile waves with material interfaces.

15. SUBJECT TERMS

16. SECURITY CLASSIFICATION OF:			17. LIMITATION OF ABSTRACT	18. NUMBER OF PAGES	19a. NAME OF RESPONSIBLE PERSON
a. REPORT **unclassified**	b. ABSTRACT **unclassified**	c. THIS PAGE **unclassified**	**Same as Report (SAR)**	**29**	

Standard Form 298 (Rev. 8-98)
Prescribed by ANSI Std Z39-18

1. Introduction

Within the present work, the problems related to the interaction of tensile stress-waves with polyurea/fused-silica and fused-silica/polyurea interfaces are analyzed. For this purpose, advanced non-equilibrium all-atom molecular-level computational methods and tools are employed. To properly account for the initial state of interfacial cohesion, and its degradation caused by the impinging tensile stress-wave, reactive forcefield potential functions (enabling dynamic and adaptive bond breaking/generation) are employed. Hence, the main aspects of the present work include: polyurea; fused silica (soda-lime glass); and reactive forcefield potentials. A brief overview of these aspects of the problem at hand is presented in the remainder of this section.

1.1 Polyurea

Polyurea falls into a class of elastomeric co-polymers which are synthesized via a fast chemical reaction between difunctional isocyanate (OCN−R′−NCO) and difunctional amine ($H_2N-R-NH_2$) precursors. The first precursor contains isocyanate ($-N=C=O$) groups and an aromatic moiety (R′) while the latter contains amine ($-NH_2$) groups and a linear hydrocarbon chain (R). The resulting single-chain molecular structure consists of alternating hard segments (HS) and soft segments (SS). A typical chemical makeup of these segments is depicted schematically in Figure 1. Examination of Figure 1 reveals the presence of two "urea linkages" per hard segment. Due to high polarity of the urea linkages, and the presence of lone electron pairs on oxygen and nitrogen atoms (the conditions which are conducive to the formation of hydrogen bonds), and possible Π-type interactions which may promote ring stacking, hard segments of the adjacent chains (or of the same chain) are subjected to strong attractive forces which promote their self-assembly/clustering. Consequently, bulk polyurea is typically not homogeneous but rather segregated, at a nanometer length scale, into the rod-shaped, so-called "hard domains." These domains are dispersed, as a discrete phase, within a continuous "soft matrix."

Hard domains contain a high glass transition temperature, T_g, hydrogen-bonded phase which controls the overall stiffness and strength of polyurea (Grujicic *et al.*, 2010a, 2011a, b, c, 2012a). On the other hand, the soft matrix consists of a low-T_g compliant phase which is responsible for the high ductility of polyurea. Typical nanometer-length-scale microstructure of polyurea as revealed using tapping-mode atomic force microscopy is shown in Figure 2 (Grujicic *et al.*, 2011b). The presence of rod-shaped hard domains is evident in this figure. Since inter-chain bonding in polyurea is mainly the result of the strong hydrogen bonding, polyurea is often referred to as being a thermoplastically cross-linked polymer. However, depending on the fraction of isocyanate functional groups with functionality (defined as the number of mer's dangling bonds, which participate in the polymerization) greater than 2.0, polyurea may also be partly cross-linked. It is established (e.g. Castagna *et al.*, 2012) that polyurea properties are greatly affected by the relative contributions of hydrogen-bonding and covalent-bonding-based cross-linking.

While polyurea has been traditionally known as a material with superior wear resistance, recent experimental and computational studies (e.g. Bogoslovov *et al.*, 2007; Grujicic *et al.*, 2010b, 2011d, 2012g) have demonstrated that this material also possesses an unusually high potential for: increasing the ballistic penetration performance of metallic and construction-material structures; and dispersion/attenuation of the shockwaves resulting from blast and/or ballistic impact loading. Recently, the potential use of polyurea as advanced combat helmet

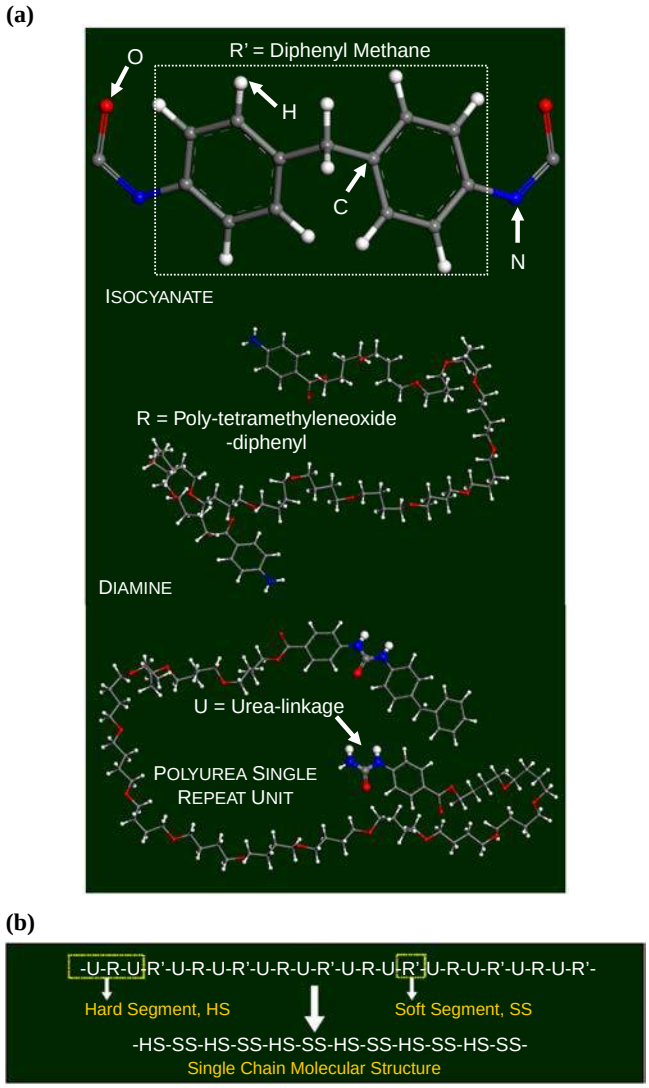

Figure 1.
(a) Co-polymerization reaction resulting in the formation of segmented polyurea; and (b) simplified notation for polyurea structure using functional groups U (urea linkage), R′ (diphenyl methane) and R″ (poly-tetramethylene-oxide-diphenyl) and the corresponding definitions of hard segments (HS) and soft segments (SS)

coating/lining and/or suspension-pad material has been explored (Grujicic *et al.*, 2010a, 2011d, 2012a, b, c, g). When used in these applications, the main role of polyurea is to mitigate blast effects and reduce undesirable consequences related to mild traumatic brain injury.

It should be noted that a clear distinction is made here between (compressive) shockwaves and (tensile) stress-waves (the subject of the present work). To explain this difference, one must first recognize that polyurea (as well as fused-silica) is an "acoustically normal" material, i.e. the wave speed increases with the extent of compression brought about by the wave loading. Consequently, under compressive loading conditions, trailing (higher compression) wavelets advance faster than their

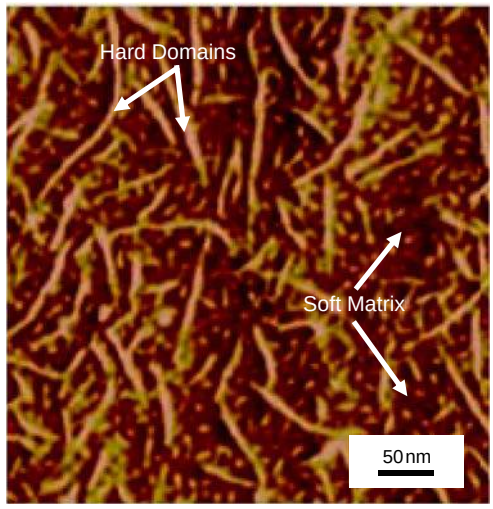

Figure 2.
An example of a typical tapping-mode atomic force microscopy (AFM) image of a polyurea showing a rod-like morphology of the hard segments

leading (lower compression) counterparts, giving rise to the formation of a (discontinuous) shockwave. In sharp contrast, in the case of tensile loading, trailing (higher tension) wavelets advance slower than their leading (lower tension) counterparts, giving rise to the formation of a continuous stress-wave with a progressively increasing front-width. While stress-waves can cause serious damage to protective structures, they have received relatively little attention in comparison to their shockwave counterparts. In fact, no reports of simulations of stress-wave generation, propagation and interaction in polyurea could be located in the open literature. On the other hand, studies have been reported concerning molecular-level analyses of shockwave phenomena in polyurea using both all-atom (Grujicic *et al.*, 2011e, 2012d) and coarse-grained (Grujicic and Pandurangan, 2012; Grujicic *et al.*, 2013a, b) non-equilibrium methods and tools. These investigations were used to: generate the basic shock-Hugoniot relations in polyurea; identify different (inelastic-deformation and energy-dissipation) phenomena/processes taking place at, or in the vicinity of, the shock front; and help elucidate the molecular-level character of these phenomena/processes.

1.2 Fused silica

Fused silica falls into the category of ceramic-glass materials. One of the basic properties of ceramic glasses (or of glasses, in general) is their lack of long-range atomic order which imparts them an amorphous microstructure. For instance, the atomic arrangement in pure silicate glass (i.e. fused silica) is highly random relative to the chemically equivalent (crystalline) quartz. To describe the structure of ceramic glasses as determined using various experimental techniques (e.g. neutron-diffraction, nuclear magnetic resonance, small angle X-ray scattering, etc.), the so-called "random network model" (Kingery *et al.*, 1976) is typically employed. Such a model represents amorphous materials as a three-dimensional linked network of polyhedra. The character (number of facets) of the polyhedra is controlled by the species-specific coordination of the central (glass-forming) atom (cation). In the case of silicate-based glasses like fused silica and soda-lime glass, the polyhedron-center atoms are all silicon and each silicon atom is surrounded by four oxygen atoms (while each oxygen atom is connected to or

bridges two silicon atoms) forming a SiO_4^{4-} tetrahedron. In glasses of different formulations, other types of polyhedra may exist. Since silicon has a tendency to form a continuous network with (bridging) oxygen atoms, SiO_2 is commonly referred to as a "network former". Other potential network formers in ceramic-glass are boron and germanium oxides.

Numerous oxides and other additives are used to modify the basic silica tetrahedra network of silicate-based glasses in order to tailor their properties to specific applications. When alkali (or alkaline earth) oxides are added to a pure silicate-based glass, in order to accommodate the excess of oxygen anions which are present due to the oxide dissociation, the continuity of the silica tetrahedra network becomes disrupted. The resulting glass structure contains additional non-bridging (connected to only one silicon atom) oxygen atoms. Charge transfer from the alkali earth metal atoms converts the non-bridging oxygen atoms into singly charged anions. The metallic cations formed in this process tend to hover around the non-bridging oxygen ions for local charge neutrality. Since alkali (or alkaline earth) based oxides cause a disruption in the continuous glass network, they are typically referred to as "network modifiers". As mentioned earlier, fused-silica ceramic glass investigated in the present work is chemically pure SiO_2 (i.e. free of glass modifiers) and contains a continuous network of Si–O bonds (i.e. it is free of non-bridging oxygen atoms).

Within the random network model, the microstructure of glass is described using several network state parameters. Among these, the most frequently used are:

(1) the so-called *R* parameter, defined as the average number of oxygen ions per network-forming ion which is used to describe the overall connectivity of a given network. In the case of fused silica, in which there are two (bridging) oxygen anions for every network-forming silicon cation, the *R* value is 2.0. In general, a larger value of the *R* parameter (brought about by the addition of network modifiers) implies a more open (less connected) weaker amorphous glass network. The effect of network formers on the *R* parameter is more complicated and depends on the network former coordination number, the strength of its bond with oxygen as well as its concentration;

(2) the so-called "*X*" parameter which defines the average number of non-bridging (connected to only a single network forming cation) oxygen atoms per network polyhedron and takes on a zero value in the case of fused silica; and

(3) the so-called "*Y*" parameter which defines the average number of bridging (connected to two network forming cations) oxygen atoms per network polyhedron and takes on a value of 4.0 in the case of fused silica.

In addition to the three parameters mentioned above, the "seemingly" random microstructure of ceramic glasses can be described using bond-length, bond-angle, pair-wise correlation, Voronoi-cell volume, etc. distribution functions. An example of the local atomic structure in fused-silica under ambient conditions is shown in Figure 3.

In addition to chemical modifications of ceramic-glass, changes in the microstructure of this material can be brought about by mechanical loading/deformation (typically requiring several GPa pressure levels). Specifically, high pressure may result in a reorganization of the atomic network (phase change) in the form of changes to the coordination of the network-forming cations. These phase changes can be of first order, which are characterized by the formation of a distinct high-pressure phase at a nominally constant pressure, or they may be of second order,

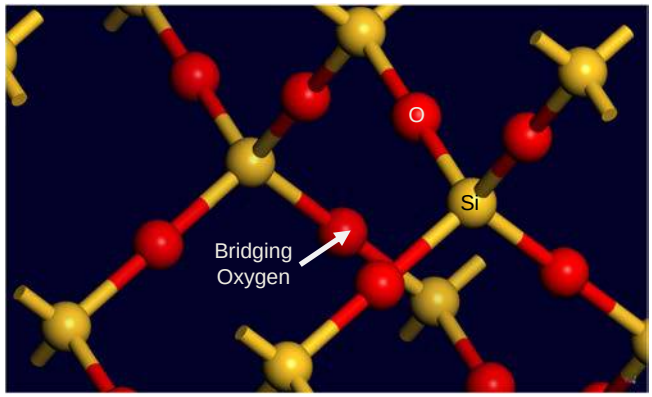

Figure 3.
An example of the local atomic structure in fused-silica

which are phase changes which involve a continuous morphing of the original phase into the final high-pressure phase over a range of pressures. In the case of fused-silica, there are first-order phase transformations were observed at pressures of 3 to 5 GPa, and involve relatively modest (3-7 percent) volume changes (Grujicic *et al.*, 2011f, g, 2012e, f). As far as the second-order phase-transformations are concerned, they are observed at substantially higher pressures (ca > 20 GPa), and are associated with substantially larger volume reductions and involve the formation of stishovite, an octahedrally coordinated glass phase (Grujicic *et al.*, 2011f, g, 2012e, f).

Examination of the open literature revealed no reports of simulations of stress-wave generation, propagation and interaction in fused-silica. On the other hand, several studies have been reported concerning all-atom molecular-level analyses of shockwave phenomena in fused-silica (e.g. Grujicic *et al.*, 2011g, h, 2012e, f). Careful examination of these studies revealed that they focus essentially on the same issues as the corresponding polyurea studies mentioned earlier.

1.3 Reactive forcefield potentials

Many engineering components are of a hybrid nature, i.e. they are made of a variety of materials, often with different types of bonding, (e.g. covalent, ionic, metallic and secondary bonding). Atomic-level analyses of the interfacial regions adjoining the constituent materials in these components is quite challenging. The most accurate methods for analyzing such interfacial regions involve quantum mechanical electronic-structure calculations. Unfortunately, quantum mechanical methods are computationally very demanding and, hence, these methods are typically limited to material systems containing no more than a few hundred interacting particles. Material systems of this size are generally too small to realistically account for the overall behavior of engineering components. While recent advances in quantum mechanical methods have enabled linear scaling between the computational cost and the material-system size, and the analysis of larger material-systems, the use of these methods remain restricted to relatively small material systems, i.e. systems which cannot accurately capture the behavior of real materials with complex microstructures.

To address the aforementioned limitations of the quantum-mechanical methods, atomic-level simulation methods were developed. In these methods, materials are described using empirically-based particle/particle interaction (forcefield potential) functions which capture the essential features of the valence-electron-based bonding

without explicitly accounting for the presence of these electrons. While, due to the empirical nature of their forcefield functions, the atomic-level methods are less accurate than their quantum-mechanical counterparts, they offer several advantages such as: substantially lower computational cost; significantly higher size of the material-systems analyzed (systems containing tens or hundreds of millions of atoms can be handled); and ability to analyze the behavior of the material-system under large mechanical and/or thermal forces. One of the major limitations of the (traditional) forcefield potentials is that their functional forms are quite different across different classes of materials (e.g. polymers, ceramics, metals, etc.), as a result of which interactions between adjoining materials with different types of bonding are typically either not accounted for, or accounted for inadequately.

To address the key limitations of the atomic-level simulation methods, in recent years new so-called reactive forcefield potentials have been introduced (e.g. van Duin *et al.*, 2001). Within the reactive forcefields, interatomic connectivity (i.e. bonding) is not predetermined, but rather is a result of dynamic and adaptive interactions between the adjacent particles. As will be presented in greater detail in the next section, the reactive forcefield potentials are developed around two basic concepts: particle self-consistent charge equilibration (an algorithm by which the atoms determine their own charges); and inter-particle bond order (defined as the "theoretical index of the degree of bonding between two atoms relative to that of a single bond, i.e. the bond provided by one localized electron pair" (IUPAC, 2013)). As in the case of the traditional (non-reactive) forcefields, the reactive forcefields include environment-dependent multi-body interactions, and are generally parameterized using the corresponding quantum-mechanical and/or experimental data. The main improvements brought about by the introduction of the reactive forcefields can be summarized as follows:

(1) while non-reactive force-fields yield reliable predictions regarding the material behavior in the states near equilibrium (while assuming constancy of the bond order and the atomic charges), the reactive forcefield enables reliable predictions of the material behavior further away from the equilibrium (e.g. in the product states resulting from chemical reactions, which generally involve bond-breaking/-generation and atomic charge changes); and

(2) furthermore, the behavior of a material system along the reaction paths, including the transition state, can be analyzed.

Unfortunately, atomic-level simulations based on the use of the reactive force-fields are associated with significantly (one to two orders of magnitude) larger computational costs. Nevertheless, these types of simulations are substantially faster than their quantum-mechanical counterparts, allowing their application to material systems containing millions of interacting particles (Chen *et al.*, 2010).

1.4 Main objective

The main objectives of the present work can be summarized as follows:

(1) to carry out an all-atom molecular-level non-equilibrium computational investigation involving reactive forcefield potentials in order to obtain the initial state of cohesion at the polyurea/fused-silica and fused-silica/polyurea material interfaces;

(2) to carry out direct all-atom molecular-level simulations of the interaction of impinging tensile stress-waves onto these material interfaces; and

(3) to determine the nature and extent of potential interfacial decohesion as a function of the impinging stress-wave strength.

1.5 Paper organization

A brief description of the reactive forcefield potential used in the present work is given in Section 2. Details regarding the all-atom molecular-level computational procedure including the computational-cell construction, forcefield identification, computational method(s) selection, stress-wave generation and the problem definition are respectively presented in Sections 3.1-3.5. The key results obtained in the present work are presented and discussed in Section 4. A summary of the key findings and concluding remarks are given in Section 5.

2. Methodology

It is well recognized that the overall utility of molecular-level computational analyses is highly affected by fidelity and accuracy of the employed force-field (a set of mathematical expressions which quantify the contribution of various bonding and non-bonding interactions between the constituents of the molecular-scale model to the material system potential energy). The present work utilizes reactive forcefield potentials. The basic structure of the reactive forcefield potentials is described in this section. The associated functional relationships will not be presented since they can be found in a number of sources (e.g. van Duin *et al.*, 2001). Within the reactive forcefield framework, the total energy of the system, E^{total} is partitioned into a number of bond-order-dependent bonding and non-bonding components as:

$$E^{total} = E^{self} + E^{Coulomb} + E^{vdW} + E^{bond} + E^{angle} + E^{torsion} + E^{conj} + E^{H-bond} + E^{lone-pair} + E^{over} + E^{under} + E^{others} \quad (1)$$

The physical meaning of the terms on the right-hand side (RHS) of Equation (1) are as follows:

(1) E^{self} is the atom-based energy term which scales with the atom charge;

(2) $E^{Coulomb}$ is the conventional electrostatic pairwise-interaction Coulomb-type energy, which includes charge-charge and nuclear charge-charge interactions. The repulsion between nuclear charges of two atoms is not covered by $E^{Coulomb}$, but is rather included in the pairwise-repulsion portion of E^{bond} (defined below). It should be noted that in contrast to common practice, Coulomb interactions (as well as van der Waals interactions, defined below) are allowed to occur between all atom pairs (within a given interaction domain, as defined by the appropriate cutoff radius). In this way, potential complications associated with the calculation of these energy terms in the case of bond breaking/generation are avoided. However, to correct for the potential orbital-overlap effects between closely spaced atoms, the so-called "shielding algorithm" is used during calculation of $E^{Coulomb}$. In addition, a seventh-order tapering function is used in the calculation of $E^{Coulomb}$ (as well as E^{vdW}) to monotonically reduce long-range interactions to zero;

(3) E^{vdW} is the van der Waals interaction energy, which includes shielding effects in order to avoid excessive repulsions between bonded atoms and atoms sharing a valence angle;

(4) E^{bond} is the bond-order-dependent energy, where the bond order quantifies the environment-dependent strength of the interaction between two bonded atoms. To enable long-range bonding necessary for accurate prediction of the chemical-reaction activation energies, bond orders are corrected in the cases when the sum of the bond orders associated with a given atom exceeds its valency (e.g. van Duin *et al.*, 2001);

(5) E^{angle} is the energy contribution associated with a two-bond angle;

(6) $E^{torsion}$ is the energy contribution associated with a three-bond torsion;

(7) E^{conj} is the energy term associated with the conjugated bond structure consisting of alternating single and multiple bonds;

(8) $E^{H\text{-}bond}$ is the hydrogen-bond term describing interactions of a hydrogen atom (bonded covalently to an atom containing a lone pair of electrons, commonly referred to as the hydrogen bond donor) within a polar molecule with another atom (commonly referred to as the hydrogen-bond acceptor);

(9) $E^{lone\text{-}pair}$ is an energy-penalty term associated with the deviation of the computed number of lone pairs on an atom from the actual number of lone pairs;

(10) E^{over} is an energy-penalty term arising from the positive deviation of the sum of the bond orders associated with an atom from its valency;

(11) E^{under} is an energy-penalty term arising from the negative deviation of the sum of the bond orders associated with an atom from its valency;

(12) E^{pen} is the penalty energy term used to reproduce the chemical stability of systems with two double bonds sharing an atom in a valency angle, as in the case of allenes;

(13) E^{triple} is the energy term that accounts for the chemical stability of the triple C–O bond, as in the case of carbon monoxide; and

(14) E^{C2} is the penalty energy term used to reduce the chemical stability of the triple C–C bond in the C2-molecule to a level comparable to that of a double bond.

It should be noted that all the energy terms appearing on the RHS of Equation (1), except for E^{vdW} and $E^{Coulomb}$ terms, depend on the bond order and vanish when the associated bond(s) are broken.

Since the reactive forcefield parameters are generally assessed using large quantum-mechanics-based training datasets, they are transferable to new material systems containing the same chemical species as the systems used in the course of parameter-identification. Sometimes, specialized reactive forcefields are developed to be used specifically for the material systems of interest. In this case, the parameter-identification procedure is shorter, since it involves fewer training datasets.

3. All-atom molecular-level computations

All-atom molecular-level computational methods and tools employed in the present work consider a material as a system of interacting (and bonded) discrete particles (i.e. atoms, ions, etc.). Furthermore, these methods and tools utilize potential-energy-minimization based (molecular statics) and Newton's second law based (molecular dynamics) algorithms to examine and quantify the behavior

and properties of the material under investigation. It is generally recognized that molecular-level computational methods and tools provide a good compromise between: ab-initio quantum mechanics methods, the methods which are intrinsically more accurate but limited to material systems containing no more than a few hundred interacting particles; and meso-scale (also known as coarse-grained) computational methods, the methods which enable analysis of larger computational domains but rely on the concept of beads, larger hypothetical particles.

In general, complete definition of a molecular-level computational model and analysis requires specification of: geometrical (e.g. atomic positions, computational-cell size, etc.) and chemical (e.g. atomic species, bond order, etc.) details of the computational model; a set of fully-parameterized force-field functions (inter-atomic potentials); and details regarding the type, the number and the usage sequence of the molecular-level computational algorithms/methods to be used in the simulation. In addition to these three aspects of the computational model/analysis, a procedure had to be introduced, in the present work, for generation of planar longitudinal tensile stress-waves within the material molecular systems. More details of these four aspects of the present computational effort, as well as of the problem analyzed in the present work, are presented in the remainder of this section.

3.1 Molecular-level computational model

As mentioned above, the primary objective of the present work is the analysis of tensile stress-wave interaction with a polyurea/fused-silica interface. Such an analysis requires generation of a polyurea/fused-silica bi-material structure. However, as will be discussed later, the stress-wave generation procedure employed in the presence of the periodic boundary conditions entailed the generation of polyurea/fused-silica/polyurea and fused-silica/polyurea/fused-silica sandwich structures. To generate such structures, molecular models for the polyurea and fused-silica subdomains are first generated and, then, they are appropriately stacked in the direction of the stress-wave propagation.

Polyurea. To construct the computational model for polyurea, the procedure developed in our prior work (Grujicic *et al.*, 2011e, 2012d) was followed. Within this procedure, a rectangular parallelepiped-shaped computational unit-cell (extended in the direction of the propagating planar stress-waves) is constructed. To prevent spurious effects associated with the presence of free-surfaces, periodic boundary conditions are imposed across the cell faces. The three edges ($a = b < c$) of the *c*ell are aligned respectively with the three global coordinate axes (x, y and z), with b being the stress-wave propagation direction. The procedure developed in Grujicic *et al.* (2011e, 2012d) involves the following steps: (a) construction of a single repeat unit; (b) construction of a single chain; (c) construction of multiple chains and their placement into the computational cell; and (d) rearrangement of the chains to obtain the necessary level of material segregation in the initial state of polyurea. Steps (a)-(b) were done using the Visualizer program from Accelrys (I), step (c) was completed using the Amorphous Cell program, also from Accelrys (II), while step (d) was executed using an in-house developed computer program. Since these details of the molecular-level computational-model construction can be found in Grujicic *et al.* (2011e, 2012d), they will not be repeated here.

Fused-silica. As in the case of polyurea, the computational model for fused-silica involves a rectangular parallelepiped-shaped computational cell, extended in the direction of stress-wave propagation and subjected to the periodic boundary condition across its faces. The three edges ($a = b < c$) of the cell are again aligned respectively

with the three global coordinate axes. To construct the computational cell for fused-silica, the procedure developed in our prior work (Grujicic *et al.*, 2011g, 2012e) was followed. This procedure involves the following steps:

(a) construction of a short silica-chain fragment, using the Visualizer program (I);

(b) growth of the fragment generated in (a) by a duplicate-and-attach process using the same program, to construct a fused-silica network structure; and

(c) packing of the fused-silica network into the computational cell using the Amorphous Cell program (II), while ensuring that the target mass density of 2.200 g/cm^3 is reached.

Polyurea/fused-silica/polyurea. To construct the computational model for the polyurea/fused-silica/polyurea sandwich structure, two polyurea computational unit-cells (described above) are used to sandwich a single fused-silica unit-cell (also described above) in the z-direction (the direction of stress-wave propagation). This procedure required that the polyurea and the fused-silica unit-cells have identical edge lengths in the x- and in the y-directions. Figure 4(a) shows a prototypical computational cell for polyurea/fused-silica/polyurea sandwich structure used in the present work. Details regarding the molecular-level structure, including bonding, in the two interfacial regions will be presented later.

Fused-silica/polyurea/fused-silica. To construct the computational model for the fused-silica/polyurea/fused-silica sandwich structure, a procedure analogous to that used to construct the polyurea/fused-silica/polyurea sandwich structure was employed. Figure 4(b) shows a prototypical computational cell for fused-silica/polyurea/fused-silica sandwich structure used in the present work. Again, details regarding the molecular-level structure, including bonding, in the two interfacial regions will be presented later.

3.2 Reactive force-field identification

The two constituent materials contain the following chemical species: (a) polyurea –C, H, O and N; and (b) fused silica – Si, O. Thus, the interfacial regions contain the following species: C, H, O, N and Si. The reactive forcefield parameters for this five-component system have been taken from Liu *et al.* (2011).

3.3 Computational methods

Two types of computational methods are employed in the present work: molecular statics; and molecular dynamics. These methods are implemented in Discover, a molecular-level simulation program from Accelrys (III).

Molecular statics. The molecular statics method is essentially a constrained-optimization technique within which the potential energy (objective function) of the computational cell (as defined by Equation (1)) is minimized with respect to the position of the constituent atoms/ions (design variables) subjected to constraints related to the imposed periodic boundary conditions. The potential energy minimization within Discover (III) is conducted by adaptively engaging and disengaging the Steepest Descent, Conjugate Gradient and the Newton's minimization algorithms. That is, the Steepest Descent method is employed in the earliest stages of the minimization procedure in order to efficiently arrive at a molecular-level configuration which is quite close to its optimum counterpart (i.e. the one associated with the minimum potential

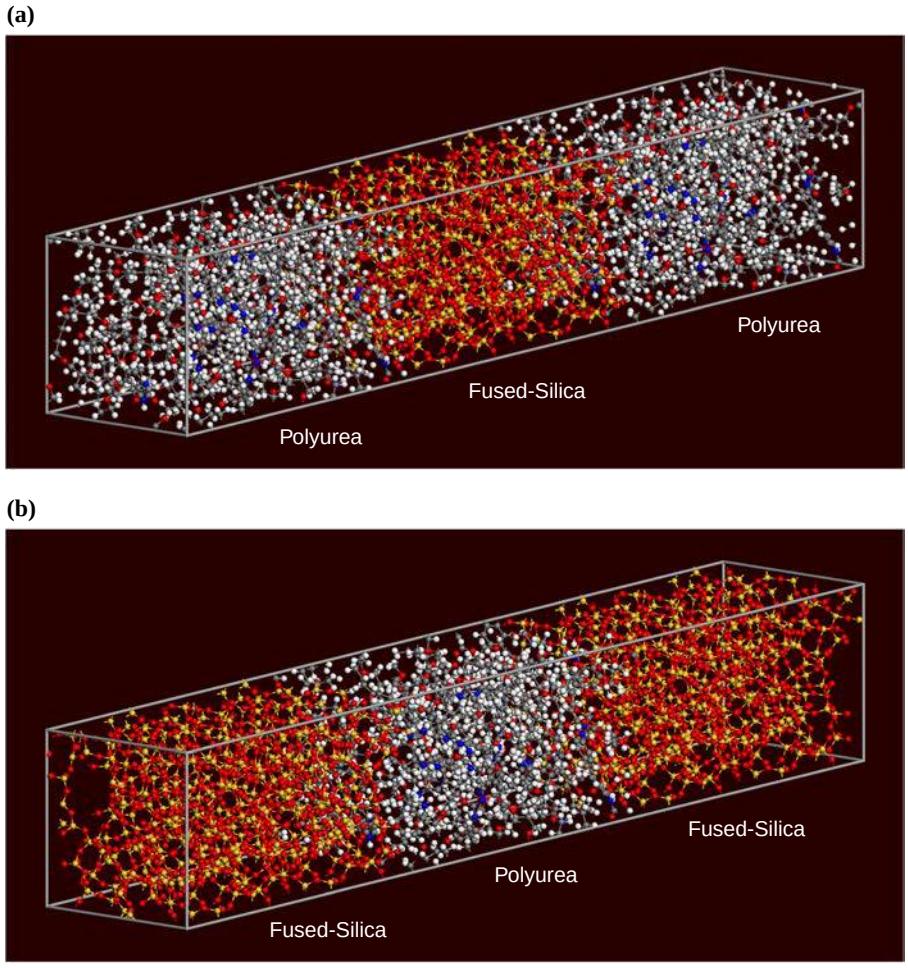

Figure 4.
Computational cells for: (a) polyurea/fused-silica/polyurea; and (b) fused-silica/polyurea/fused-silica sandwich structures

energy). On the other hand, in the latest stages of the minimization procedure, the Newton's algorithm is employed which ensures a monotonic and stable transition of the material into its optimal configuration.

Molecular statics is employed to minimize the potential energy of the newly constructed computational cells (described in Section 3.1). In addition, as will be discussed in greater detail in Section 4, this method is also employed to help quantify the state of the material swept by a stress-wave.

Molecular dynamics. Within the molecular dynamics method, negative gradient of the potential energy evaluated at the location of each atom is first used to compute forces acting on each atom. Then, the associated Newton's equations of motion (three equations for each atom) are integrated numerically with respect to time in order to determine the temporal evolution of the material molecular-level configuration. Molecular dynamics methods are generally classified into the equilibrium and non-equilibrium methods, and both of these methods are employed in the present work.

Within the equilibrium molecular-dynamics methods, the subject material system is maintained in the state of thermal-mechanical equilibrium by coupling it to the surroundings, such as a constant pressure bath, a constant temperature reservoir, etc. This ensures the absence of net flux of the mass, momentum and energy in any of the three principal coordinate directions. In the present work, NVT (where N is the (fixed) number of atoms, V, the computational-cell volume (also fixed), and T ($=298$ K) is the temperature) equilibrium molecular dynamics is employed in the first stage of the shock generation procedure (more details of this procedure will be provided in the next section).

Within non-equilibrium molecular dynamics, the system is subjected to large mechanical and/or thermal perturbations (finite changes in the axial parameter of the computational cell, in the present case). As a consequence, the system experiences large fluxes of its thermodynamic quantities (mass, momentum and energy, in the present case). Since Discover was initially designed to carry out equilibrium molecular-dynamics simulations, a procedure had to be devised to deactivate "equilibration" portions of this algorithm so that non-equilibrium molecular-dynamics calculations can be carried out.

3.4 Generation of molecular-level stress-waves

Since the materials analyzed in the present work are of a bulk type (which was accomplished through the use of periodic boundary conditions), molecular-level tensile stress-waves could be generated only in pairs (i.e. two shocks per unit cell). The procedure employed in the present work to generate molecular-level tensile stress-waves, relies on a step-wise sequential expansion of the computational-cell longitudinal lattice parameter, c.

To generate a pair of converging tensile stress-waves within the unit cell, the following procedure is employed: first, before the stress-waves are introduced, a "sufficiently long" NVT molecular dynamics simulation is conducted in order to thermally equilibrate the system at its target temperature (298 K); second, the thermal-equilibration algorithm is disabled in order to allow Discover to run in a non-equilibrium molecular-dynamics mode; third, the stress-waves are then initiated (and driven) by continuously expanding the computational-cell longitudinal lattice-parameter c as:

$$c(t) = c(t = 0) + 2u_p t \tag{2}$$

where t denotes time and u_p is the desired/pre-selected particle velocity (of the material swept by either of the shock waves) in the z-direction. In the present work, u_p is varied in a -200 to $-1{,}000$ m/s range in order to simulate the generation and propagation of tensile stress-waves of various strengths; and (d) during the application of the stress-wave-generation procedure, computational-cell transverse lattice parameters a and b are kept constant in order to obtain planar, longitudinal (i.e. uniaxial-strain) stress conditions.

The molecular-level tensile stress-wave-generation procedure described above results in the formation of two converging identical tensile stress-waves (at the computational-cell longitudinal faces), each moving towards the computational-cell center at a shock speed U_s. The passage of these tensile stress-waves through the material causes an abrupt and substantial decrease in the material mass density, as well as an increase in the internal-energy density, stress, and (absolute value of) particle velocity. Furthermore, interactions of these tensile stress-waves with the polyurea/fused-silica and fused-silica/polyurea material interfaces results in the formation of transmitted

stress-waves and reflected stress-/release-waves, and may also lead to interfacial decohesion.

The aforementioned procedure for molecular-level stress-wave generation, including the initial thermal-equilibration molecular-dynamics based procedure, is conducted through the use of a Discover input file (III). This file is written using the Basic Tool Command Language (BTCL) which enabled the use of a scripting engine that provides very precise control of simulation tasks, e.g. sequential expansion of the computational cell in the longitudinal direction, deactivation of the thermal-equilibration algorithm during the stress-wave-generation process, etc.

3.5 Problem formulation

The problem addressed in the present work can be summarized as follows: first, the computational procedures described in the previous sections are used to construct molecular-level computational cells and the resident converging tensile stress-waves of various strengths; second, the material-configuration/dynamics results are then used in a post-processing computational procedure in order to analyze the outcome of the interaction of the incident stress-waves with the material boundaries in question; and third, a detailed microstructural investigation of the interfacial regions prior to and following the incident- stress-wave/material-boundary interaction was conducted to provide additional insight into the outcome of the stress-wave/interface interactions.

4. Results and discussion

The main emphasis of this section is the presentation and discussion of the results pertaining to the interaction of tensile stress-waves with polyurea/fused-silica and fused-silica/polyurea interfaces. However, before these results are presented, a few important results obtained by extending our analysis presented in Grujicic *et al.* (2014c) are overviewed and discussed. These results are important from the standpoint of predicting and rationalizing the outcome of the tensile stress-wave interaction with the material interfaces in question.

4.1 Stress/particle-velocity/mass-density/wave-speed relationships

Using the post-processing procedure based on the concept of so-called Lagrangian bins (Grujicic *et al.*, 2014c), the basic functional relationships are obtained between the uniaxial-strain tensile stress, particle velocity, material mass density, and the speed of the wave-characteristics. These relationships are depicted in Figures 5(a)-(d) for polyurea and 6(a)-(d) for fused-silica. Examination of the results depicted in these figures shows that both polyurea and fused-silica behave as "normal" materials under tensile loading conditions. That is, as the intensity of the tensile stress-wave is increased (as quantified by an increase in the tensile stress and the particle-velocity magnitude, and by a decrease in the material mass density), the associated stress-wave acquires a lower speed. Consequently, a tensile stress-wave tends to spread (i.e. the leading-characteristic/trailing-characteristic distance increases) as it propagates through polyurea and fused-silica.

4.2 Application of the impedance-matching procedure

In this section, a brief overview is provided of the so-called impedance-matching procedure (Grujicic *et al.* 2013c, 2014b), which is used to predict the outcome of the interaction of the tensile stress-wave with the polyurea/fused-silica and fused-silica/polyurea material interfaces.

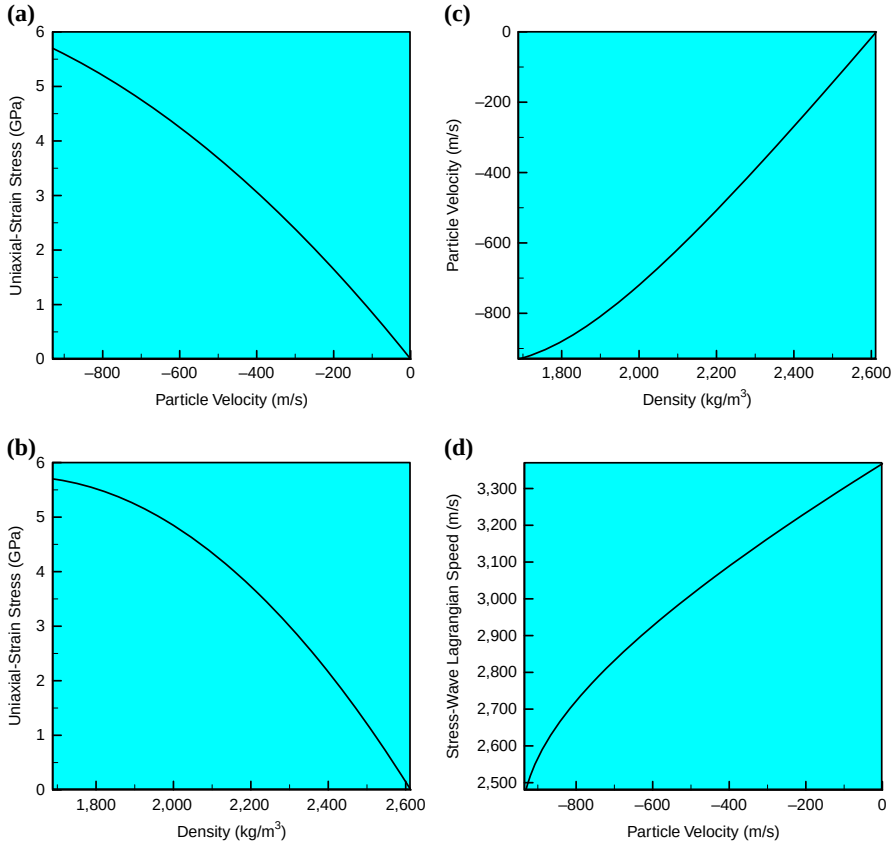

Notes: (a) Longitudinal stress, t_{11} vs particle velocity, u_p; (b) t_{11} vs material mass density, ρ; (c) u_p vs ρ; and (d) stress-wave Lagrangian speed, U_w vs u_p

Figure 5.
All-atom molecular-level computational-analysis-based relationships in polyurea:

Polyurea/fused-silica interface. The impedance-matching procedure utilizes the functional relationships between the tensile stress, t_{11}, and the particle velocity, u_p, for the two materials in question. This type of relation is used since the interaction of a stress-wave with the material boundary results in the formation of a transmitted stress-wave and a reflected stress- or release-wave, while ensuring that the stress and the particle velocities remain continuous across the material boundary. To help explain the impedance-matching method, t_{11} vs u_p relations for polyurea and fused-silica are depicted (using solid lines) in Figure 7(a). It should be noted that due to the fact that only the right-propagating tensile-stress-wave is analyzed, the particle velocities are negative. Also, due to the tensile nature of the stress-wave, t_{11} takes on positive values. In other words, the bottom right corner of the plot displayed in Figure 7(a) corresponds to the zero-particle-velocity/zero-stress condition. As one moves to the left, the particle velocities become more negative, while as one moves upward, the stress takes on more positive values. The states of the polyurea swept by one of the (right-propagating) stress-wave characteristics and the stress-free quiescent fused-silica material, before the wave-characteristic in question interacts with the polyurea/fused-silica interface,

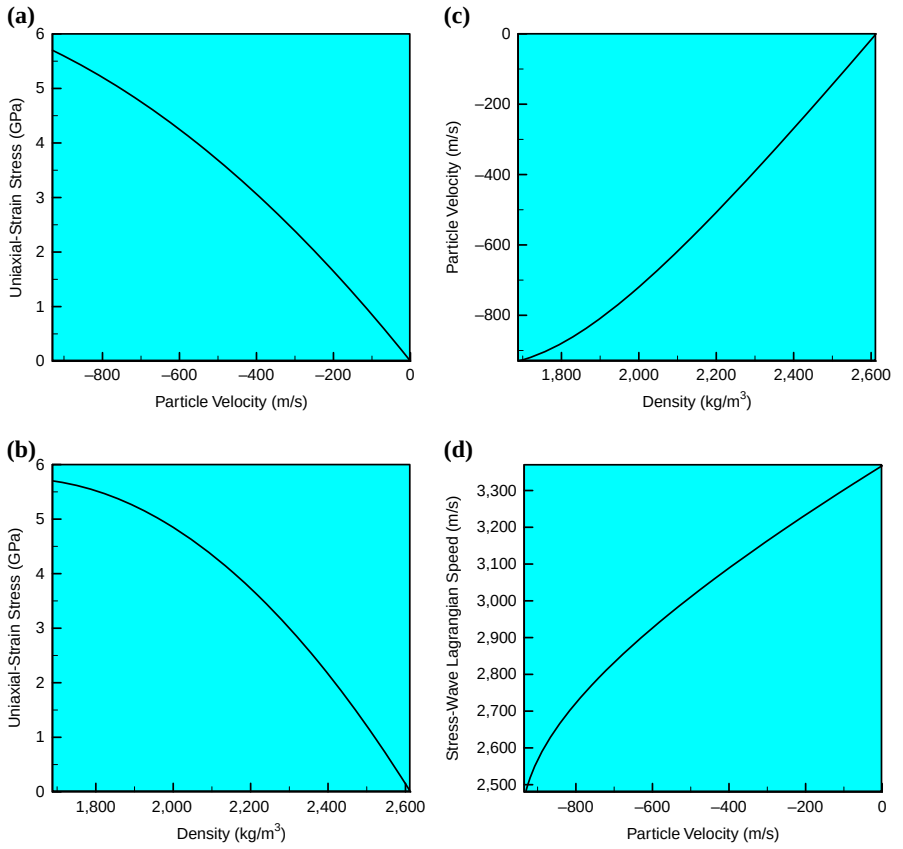

Figure 6.
All-atom molecular-level computational-analysis-based Hugoniot relations in fused-silica

Notes: (a) Longitudinal stress, t_{11} vs particle velocity, u_p; (b) t_{11} vs material mass density, ρ; (c) u_p vs ρ; and (d) stress-wave Lagrangian speed, U_w vs u_p

are denoted by a filled square (labeled *A*) and triangle (labeled *B*), respectively. After the interaction of the characteristic in question with the material interface, the state of the interfacial region is obtained by:

(1) mirroring the polyurea t_{11} vs u_p curve about a vertical constant-u_p line (where u_p is associated with the wave characteristic in question). The result of this exercise is depicted in Figure 7(a) using a dashed line; and

(2) the intersection of the mirrored polyurea curve with the fused-silica curve defines the states of the interfacial region after the interaction of the characteristic in question with the material interface, point *C* in Figure 7(a).

A comparison of the material state corresponding to point *C* with those corresponding to the material states *A* and *B*, and recognition of the facts that: first, the transmitted wave propagates in the same direction as the incident wave; second, the reflected wave propagates in the opposite direction; and third, the polyurea and fused-silica t_{11} vs u_p curves are located in the region associated with negative u_p and positive t_{11}, reveals that a right-propagating transmitted stress-wave is generated in the fused-silica and a

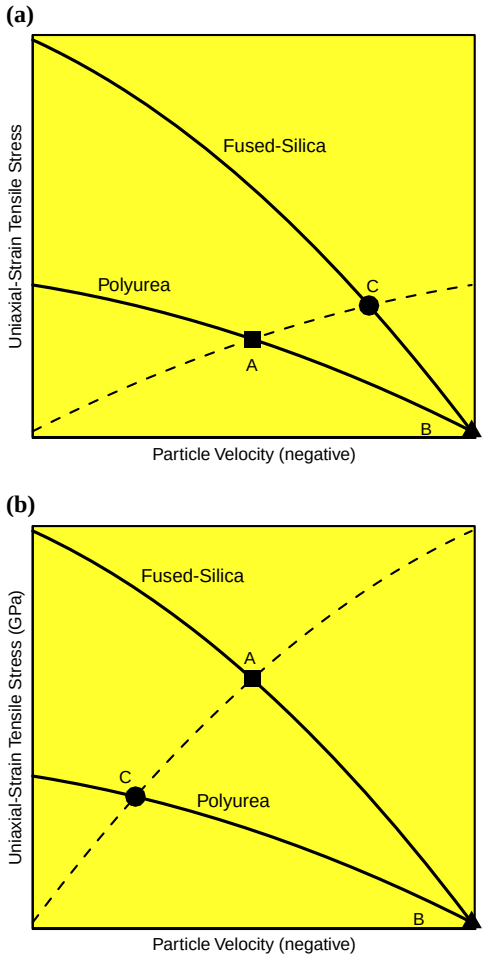

Figure 7.
Impedance-matching procedure used to determine the outcome of the interaction of an incident stress-wave in: (a) polyurea with the polyurea/fused-silica interface; and (b) fused-silica with the fused-silica/polyurea interface. Please see text for explanation of the labeled points and dashed lines

left-propagating reflected re-stress-wave (i.e. a wave which further increases the tensile stress) is generated in the polyurea. It is the fact that the magnitude of t_{11} increases in the two materials, as a result of the interaction of the incident stress-wave with the material boundary, that defines the stress-/re-stress character of the transmitted and reflected waves. Also, since the polyurea is re-stressed by a left-propagating wave, there is an accompanying decrease in the magnitude of the (negative) u_p.

Application of the procedure described above, and the results depicted in Figures 5(a)-(d) and 6(a)-(d), to the problem of interaction of an incident stress-wave within polyurea with the polyurea/fused-silica interface, is shown in Figure 8(a)-(f), the results labeled "Impedance-matching." In Figure 8, parts (a), (c) and (e) correspond to the state of the polyurea/fused-silica bi-material before the interaction, while parts (b), (d) and (f) correspond to the state of the same bi-material after the interaction. Three state/kinematic variables are monitored in these figures: particle velocity; stress; and mass density.

Examination of the results labeled "Impedance-matching" in Figure 8(a)-(f) reveals that the interaction of an incident polyurea-resident stress-wave with the

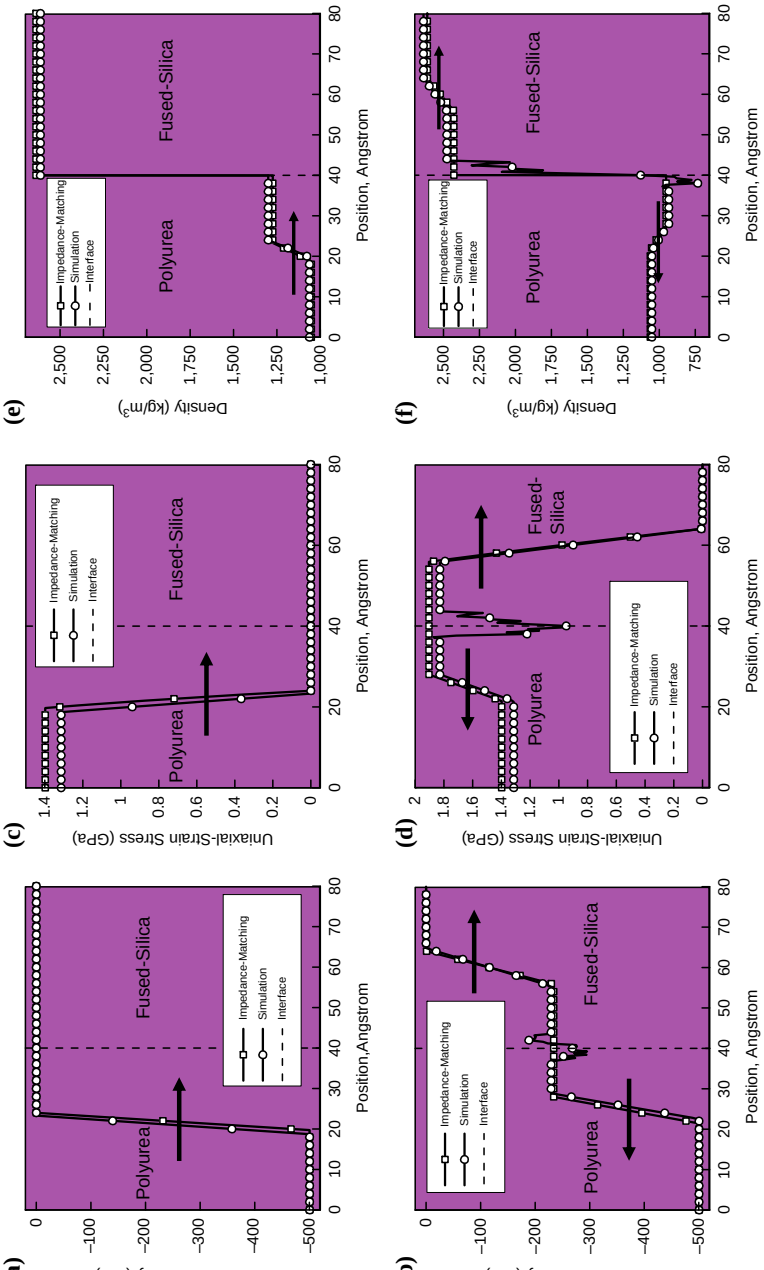

Notes: (a)-(b), Axial stress, (c)-(d) and mass density, (e)-(f) along the length of the polyurea/fused-silica bi-material before, (a), (c), (e) and after, (b), (d), (f) the interaction of the incident stress-wave residing in polyurea with the polyurea/fused-silica boundary. Please see text for details

Figure 8.
Distribution of the particle velocity

polyurea/fused-silica boundary: creates a transmitted right-propagating stress-wave which imparts negative particle velocity and tensile stress to the "stressed" fused-silica, while decreasing the mass density of this material; and creates a reflected left-propagating re-stress-wave which decreases the magnitude of the particle velocity, increases the tensile stress and decreases the mass density of the swept polyurea.

Fused-silica/polyurea interface. The aforementioned impedance-matching procedure is also utilized in the case of the fused-silica/polyurea interface. In this case, t_{11} vs u_p relations for polyurea and fused-silica are depicted (using solid lines) in Figure 7(b). The states of the (stressed) fused-silica swept by one of the stress-wave characteristics and the stress-free quiescent polyurea material, before this characteristic right-propagating stress-wave interacts with the fused-silica/polyurea interface, are denoted by a filled square (labeled A) and triangle (labeled B), respectively. After the interaction of the wave characteristic in question with the material interface, the state of the interfacial region is obtained by:

(1) mirroring the fused-silica t_{11} vs u_p curve about a vertical constant-u_p line (associated with the wave characteristic in question). The result of this exercise is depicted in Figure 7(b) using a dashed line; and

(2) the intersection of the mirrored fused-silica curve with the polyurea curve defines the states of the interfacial region at the time of the interaction of the wave characteristic with the fused-silica/polyurea interface, point *C* in Figure 7(b).

A comparison of the material states corresponding to point *C* with those corresponding to the material states *A* and *B*, recognition of the fact that u_p is negative, and the orientation of the polyurea and fused-silica t_{11} vs u_p curves passing through point *C* reveal that: a right-propagating transmitted stress-wave is generated in the polyurea; and a left-propagating reflected release-wave is generated in the fused-silica. It is the fact that the magnitude of t_{11} decreases in the fused-silica as a result of the interaction of the incident stress-wave with the material boundary, that defines the release-wave character of the reflected wave. Also, since the pre-stressed fused-silica is relaxed by the passage of the release-wave, there is an accompanying increase in the (negative) u_p in this material.

Application of the procedure described above, to the problem of interaction of an incident stress-wave within fused-silica, with the fused-silica /polyurea interface, is shown in Figure 9(a)-(f). In Figure 9, parts (a), (c) and (e) correspond to the state of the fused-silica/polyurea bi-material before the interaction, while parts (b), (d) and (f) correspond to the state of the same bi-material after the interaction. The same three state/kinematic variables, as in the case of Figure 8(a)-(f), are monitored in Figure 9(a)-(f), the results labeled "Impedance-matching."

Examination of the results labeled "Impedance-matching" in Figure 9(a)-(f) reveals that the interaction of an incident fused-silica-resident stress-wave with the fused-silica/polyurea boundary: creates a transmitted right-propagating stress-wave which imparts negative particle velocity and tensile stress to, while decreasing the mass density of, the "stressed" polyurea; and creates a left-propagating release-wave which increases the magnitude of the particle velocity, decreases the tensile stress and increases the mass density of the swept fused-silica.

4.3 Simulation of the stress-wave/material-boundary interactions

In this subsection, the all-atom simulation results pertaining to the interaction of an incident polyurea- or fused-silica-resident stress-wave with a polyurea/fused-silica or

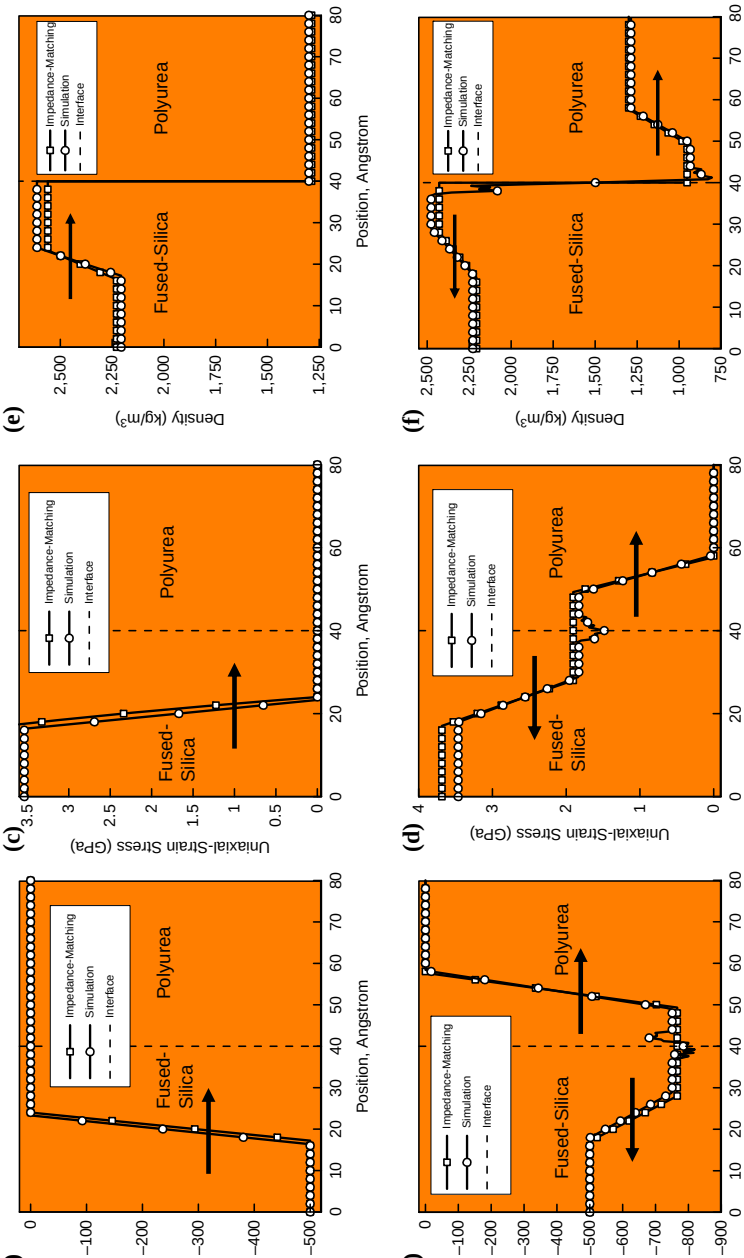

Figure 9.
Distribution of the particle velocity

Notes: (a)-(b), Axial stress, (c)-(d) and mass density, (e)-(f) along the length of the fused-silica/polyurea bi-material before, (a), (c), (e) and after, (b), (d), (f) the interaction of the incident stress-wave residing in fused-silica with the fused-silica/polyurea boundary. Please see text for details

fused-silica/polyurea boundary are presented and discussed. Special attention is paid to revealing spatial distribution and temporal evolution of the particle velocity, stress, and mass density prior to and after the stress-wave/material-boundary interaction.

Polyurea/fused-silica interface. It should be recalled that in the case of the results labeled "Impedance-Matching" in Figure 8(a)-(f), the impedance-matching method was used, in conjunction with the all-atom-simulation-derived functional relationships between the stress, particle velocity, mass density and the wave speed. In this section, the impedance-matching method was not used. Instead, the previously mentioned Lagrangian-bin method was combined with the virial theorem (Grujicic *et al.*, 2014a) and applied within a post-processing procedure to the all-atom-simulation results to determine the spatial distribution and temporal evolution of the particle velocity, stress, and mass density prior to and after the stress-wave/material-boundary interaction. The results obtained using this procedure, labeled "Simulation," are depicted in Figure 8(a)-(f).

A comparison of the corresponding "Impedance-Matching" and "Simulation" results displayed in Figure 8(a)-(f) reveals:

(1) before the interaction of the incident polyurea-resident stress-wave with the polyurea/fused-silica interface, the location and shape of the stress-wave (as represented by the spatial distribution of the particle velocity, stress and mass density) are in fairly good agreement with their impedance-matching-based counterparts, Figure 8(a), (c) and (e); and

(2) as in the case of the "Impedance-Matching" results, the "Simulation" results show the formation of a transmitted right-propagating stress-wave and a reflected left-propagating re-stress-wave upon the interaction of the incident polyurea-resident shockwave with the polyurea/ fused-silica interface, Figure 8(b), (d) and (f). However, the two sets of results considered show more differences than in the case of the incident stress-wave. Specifically, while continuity in the particle velocity and stress appears to be maintained in the case of the "Simulation-based" results, these results are quite irregular in the interfacial region. Further away from the interfacial region, the "Simulation" results tend to reacquire their "well-behaved" character. These findings suggest that, perhaps, the interaction of the incident stress-wave with the polyurea/ fused-silica interface gives rise to some form of microstructural changes in the interfacial region.

Fused-silica/polyurea interface. The results obtained in this portion of the work (labeled as "Simulation" in Figure 9(a)-(f)) are again obtained by combining the Lagrangian-bin method with the virial theorem and the method for determination of the particle number-density.

A comparison of the corresponding "Impedance-Matching" and "Simulation" results displayed in Figure 9(a)-(f) reveals that:

(1) before the interaction of the incident fused-silica-resident stress-wave with the fused-silica/polyurea interface, the location and shape of the stress-wave (as represented by the spatial distribution of the particle velocity, stress and mass density) are in fairly good agreement with their impedance-matching-based counterparts, Figure 9(a), (c) and (e); and

(2) as in the case of the "Impedance-Matching" results, the "Simulation" results show the formation of a transmitted right-propagating stress-wave and a

reflected left-propagating release-wave upon the interaction of the incident fused-silica-resident shockwave with the fused-silica/polyurea interface, Figure 9(b), (d) and (f). However, the two sets of results considered show more differences than in the case of the incident stress-wave. In particular, while continuity in the particle velocity and stress appears to be maintained in the case of the "Simulation-based" results, these results are quite irregular in the interfacial region. Further away from the interfacial region, the "Simulation" results tend to reacquire their "well-behaved" character. These findings suggest that, perhaps, the interaction of the incident stress-wave with the fused-silica/polyurea interface gives rise to some form of microstructural changes in the interfacial region.

4.4 Stress-induced changes in the interfacial-region microstructure

In this subsection, the all-atom simulation results pertaining to the interaction of an incident polyurea- or fused-silica-resident stress-wave with a polyurea/fused-silica or fused-silica/polyurea boundary are presented and discussed. Special attention is paid to revealing the changes experienced by the interfacial region after its interaction with the incident stress-wave.

Polyurea/fused-silica interface. The results presented in the previous section suggested the possibility of microstructural changes in the polyurea/fused-silica interfacial region as a result of the stress-wave interaction with the interface. In this section, the results obtained after the examination of the material microstructure in the polyurea/fused-silica interfacial region are presented and discussed. Figure 10(a) shows a relatively thin slice of the molecular structure of the polyurea/fused-silica bi-material prior to the arrival of the incident polyurea-resident stress-wave. Examination of this figure reveals the presence of a thin interfacial region within which bonding is established between the two adjoining materials. The same interfacial region following the interaction of the incident polyurea-resident stress-wave within the polyurea/fused-silica interface is depicted in Figure 10(b). Careful examination of the molecular structure displayed in this figure and its comparison with the results displayed in Figure 10(a) reveals that the interfacial region has undergone some microstructural changes as a result of its interaction with the incident stress-wave. Specifically, it is seen that some of the trans-interface bonds have been broken and that the two adjoining materials have undergone some decohesion/detachment. These microstructural changes can then be used to explain the aforementioned differences between the "Impedance-Matching" and "Simulation" results in the interfacial region, as observed in Figure 8(b), (d) and (f).

Fused-silica/polyurea interface. In this section, the results yielded by the examination of the material microstructure in the fused-silica/polyurea interfacial region are presented and discussed. Figure 11(a) shows a relatively thin slice of the molecular structure of the fused-silica/polyurea bi-material prior to the arrival of the incident fused-silica-resident stress-wave. Examination of this figure again reveals the presence of a thin interfacial region within which bonding is established between the two adjoining materials. The same interfacial region following the interaction of the incident fused-silica-resident stress-wave within the fused-silica/polyurea interface is depicted in Figure 11(b). Careful examination of the molecular structure displayed in this figure and its comparison with the results displayed in Figure 11(a) reveals that the interfacial region has undergone some microstructural changes as a result of its

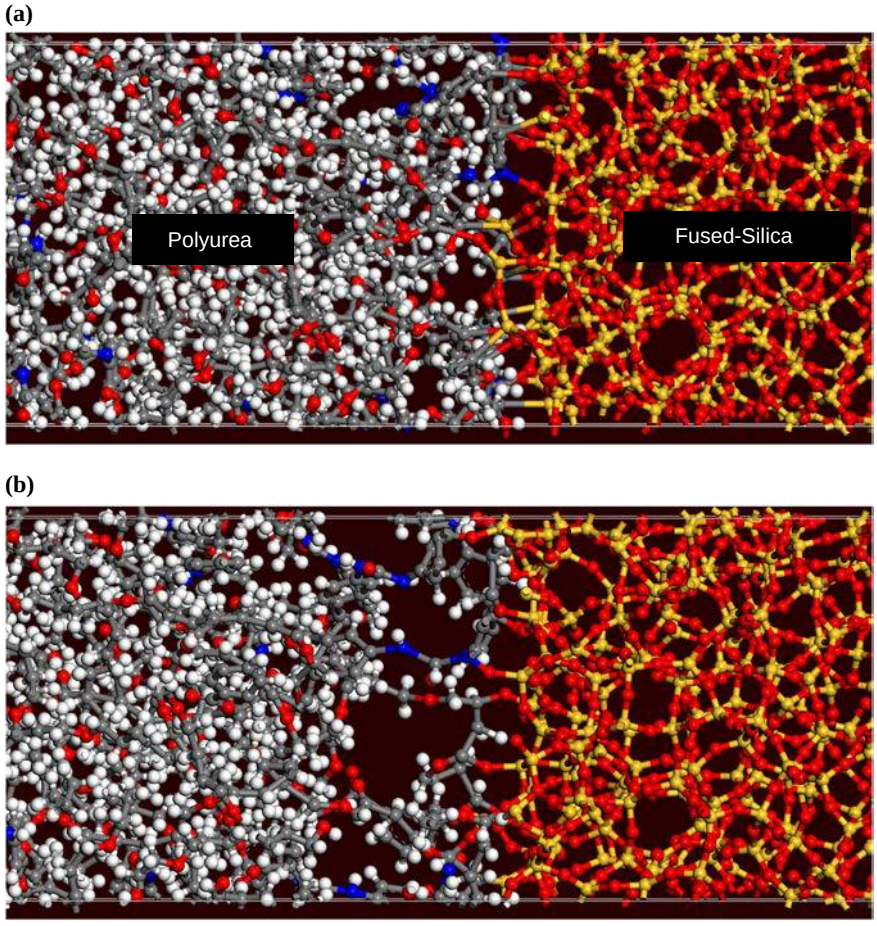

Notes: (a) Before; and (b) after the arrival of the polyurea-resident right-propagating incident stress-wave to, and its interaction with, the polyurea/fused-silica interface

Figure 10.
An example of the molecular-level microstructure in the polyurea/fused-silica bi-material

interaction with the incident stress-wave. Specifically, it is seen that some of the trans-interface bonds have been broken and that the two adjoining materials have undergone some decohesion/detachment. The extent of these microstructural changes is lower than that observed in the case of the interaction of the incident polyurea-resident stress-wave with the polyurea/fused-silica interface, Figure 10(b). This finding can be rationalized by the fact that while the intensity of the incident stress-waves (as measured by the peak-stress values) is identical in both stress-wave/interface interaction-cases, the reflected stress-wave in the case of Figure 10(b) is of a re-stress character (i.e. causes an increase in the interfacial stress), while the reflected stress-wave in the case of Figure 11(b) is of a release character (i.e. causes an decrease in the interfacial stress). In other words, the tensile stress experienced by the polyurea/fused-silica interface is larger than its counterpart in the fused-silica/polyurea case. Consequently, a larger extent of interfacial decohesion is

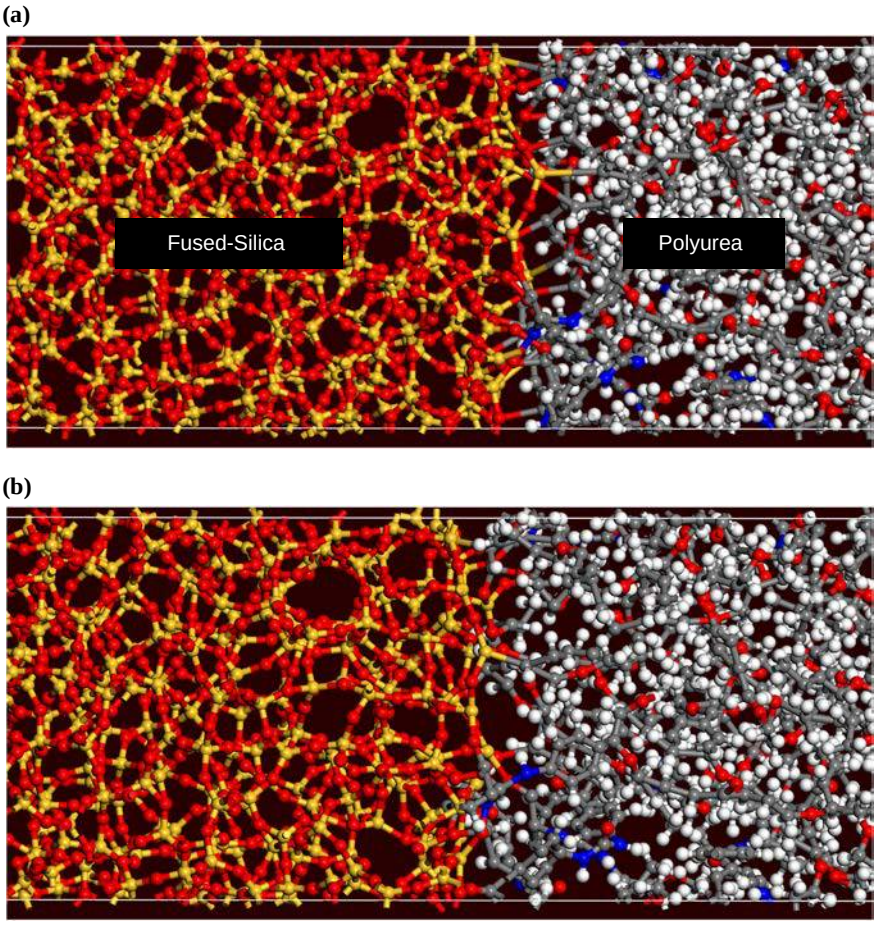

Figure 11.
An example of the molecular-level microstructure in the fused-silica/polyurea bi-material

Notes: (a) Before; and (b) after the arrival of the fused-silica-resident right-propagating incident stress-wave to, and its interaction with, the fused-silica/polyurea interface

observed in the former than in the latter case. It should be further noted that although the extent of microstructural changes is lower in the fused-silica/polyurea interface case, these changes are of a sufficiently large magnitude to affect spatial distribution and temporal evolution of the particle velocity, stress and mass density, Figure 9(b), (d) and (f).

4.5 Experimental validation

The work presented in this manuscript is of a purely computational nature. Examination of the public-domain literature did not reveal any experimental results pertaining to the interaction of the tensile stress-waves with the polyurea/fused-silica or fused-silica/polyurea material interfaces which could be used to validate the present computational analysis. Nevertheless, available related experimental results can be used to judge the overall soundness of the findings obtained in the present work.

The two main reasons that the polyurea/fused-silica system was investigated in the present work are:

(1) polyurea is being considered as a durable adhesive in ship-building applications, providing good resistance to high-intensity static and dynamic loads (e.g. those arising from underwater blasts and ocean waves). In these applications, polyurea/glass interfaces can be encountered in the case of portholes, where polyurea is used as an adhesive/sealant for the glass disks; and

(2) while polyurea as an adhesive in ship-building applications is more frequently used to join stainless steel to glass-reinforced composites, no reliable reactive force-fields are presently available for these material systems to be analyzed using all-atom molecular-level calculations.

Since the present computational work reveals interfacial decohesion under dynamic loading conditions, the relevant experimental results must also be related to the problem of interfacial decohesion under dynamic loading conditions. Examination of the open-domain literature revealed that, perhaps, the so-called "laser spallation tests" generate experimental results which are most closely related to the computational results which can be generated using the present all-atom molecular-level simulations.

The basic principle behind the laser spallation experiment can be found in a series of papers by Gupta and co-workers (e.g. Pronin and Gupta, 1998; Wang and Gupta, 2006; Kim *et al.*, 2012). In short, the laser spallation experiments involve:

(1) the basic test sample is a structure consisting of a thin polyurea middle layer sandwiched between two plates of the materials (e.g. steel and glass-reinforced composite) whose interfacial strengths with polyurea are being investigated. One of the end faces of the test sample is coated with an approximately 1.0-μm-thick sputtered aluminum and subsequently overcoated with 40-50-μm-thick waterglass (hydrated SiO_2). Upon dehydration of the water-glass layer, the aluminum layer becomes constrained by SiO_2;

(2) next, an approximately 4-mm-diameter area on the aluminum film is impinged by a (typically 2.5-ns Nd:YAG) laser pulse;

(3) localized laser-induced melting of the aluminum under confinement produces a (typically a 1 ns rise time) compressive stress pulse into the adjoining plate material;

(4) the incident stress-wave travels through the first plate to the first-plate/polyurea interface, where it partially transmits and partially reflects. The transmitted compressive stress-wave within polyurea travels through the polyurea/second-plate interface, where it again partially transmits and partially reflects. The transmitted compressive stress-wave within the second plate propagates to the back-face free surface, where it reflects as a tensile wave. Provided this tensile wave is of sufficient strength, it can cause decohesion at the weaker of the two interfaces involving polyurea;

(5) the intensity of the reflected tensile wave can be controlled by varying the fluence of the incident laser beam while keeping the impingement area constant. This procedure enables determination of the critical fluence at which the interfacial decohesion is first detected (using a post-mortem optical microscopy examination);

(6) next, the critical laser fluence has to be correlated with the peak stress present in the reflected tensile wave. Towards that end, a new test sample is constructed in which the polyurea and the second plate are not used. The laser-illumination experiment under the critical-fluence conditions is then carried out and the interferometry at the back-face of the first plate is used to determine the time-resolved profile of the incident compressive wave; and

(7) then the finite element analysis of the interaction of this stress-wave with the first-plate/polyurea interface, the interaction of the transmitted stress-wave with the polyurea/second-plate interface, and the interaction of the second transmitted wave with the second-plate back-face free-surface is conducted in order to determine the peak stress in the reflected tensile stress-wave.

The laser spallation experiments involving polyurea middle layers typically yielded interfacial-strength levels in the 50-250 MPa range (depending on the nature of the adjoining plate materials). The present computational results reveal the polyurea/fused-silica interfacial strength in the 90-110 MPa range, which is comparable to its experimentally determined counterpart. This finding suggests that the employed all-atom computational analysis has the potential to reveal the intrinsic cohesion-resistance of different material interfaces, provided high-fidelity reactive force-fields are available for the material systems in question.

5. Summary and conclusions

Based on the results obtained in the present work, the following summary remarks and main conclusions can be drawn:

(1) molecular-level computational methods and tools are used to analyze the interaction of tensile stress-waves with polyurea/fused-silica and fused-silica/polyurea material interfaces;

(2) the results related to the propagation of the stress-waves within polyurea and fused-silica are used to determine functional shock-Hugoniot relationships between the uniaxial-strain stress, particle velocity, mass density and the stress-wave speed;

(3) interaction of sufficiently strong incident polyurea- or fused-silica-resident tensile stress-waves with the corresponding interface has been found to give rise to microstructural changes involving interfacial bond-breaking and decohesion;

(4) these microstructural changes are found to alter the characteristics of the transmitted stress-waves and the reflected stress-/release-waves at the material interfaces in question; and

(5) while no experimental results for the polyurea/fused-silica cohesion-strength are presently available, the computed cohesive-strength results obtained in the present work are found to be in the physically realistic range, and to be consistent with their experimental counterparts involving polyurea adjoined to another (non-fused-silica) material.

References

Bogoslovov, R.B., Roland, C.M. and Gamache, R.M. (2007), "Impact-induced glass transition in elastomeric coatings", *Applied Physics Letters*, Vol. 90 No. 22, pp. 221910-1-221910-3.

Castagna, A.M., Pangon, A., Choi, T., Dillon, G.P. and Runt, J. (2012), "The role of soft segment molecular weight on microphase separation and dynamics of bulk polymerized polyureas", *Macromolecules*, Vol. 45 No. 20, pp. 8438-8444.

Chen, H.-P., Kalia, R.K., Kaxiras, E., Lu, G., Nakano, A., Nomura, K.I., van Duin, A.C.T., Vashishta, P. and Yuan, Z. (2010), "Embrittlement of metal by solute segregation-induced amorphization", *Physical Review Letters*, Vol. 104 No. 15, p. 155502.

Grujicic, M. and Pandurangan, B. (2012), "Meso-scale analysis of segmental dynamics in micro-phase segregated polyurea", *Journal of Materials Science*, Vol. 47 No. 8, pp. 3876-3889.

Grujicic, M., He, T. and Pandurangan, B. (2011a), "Development and parameterization of an equilibrium material model for segmented polyurea", *Multidiscipline Modeling in Materials and Structures*, Vol. 7 No. 2, pp. 96-114.

Grujicic, M., Bell, W.C., Pandurangan, B. and Glomski, P.S. (2011d), "Fluid/structure interaction computational investigation of the blast-wave mitigation efficacy of the advanced combat helmet", *Journal of Materials Engineering and Performance*, Vol. 20 No. 6, pp. 877-893.

Grujicic, M., Bell, W.C., Pandurangan, B. and He, T. (2010a), "Blast-wave impact-mitigation capability of polyurea when used as helmet suspension pad material", *Materials and Design*, Vol. 31, pp. 4050-4065.

Grujicic, M., Snipes, J.S., Galgalikar, R. and Ramaswami, S. (2014b), "Material-model based determination of the shock-hugoniot relations in nanosegregated polyurea", *Journal of Materials Engineering and Performance*, Vol. 23 No. 2, pp. 357-371.

Grujicic, M., Ramaswami, S., Snipes, J.S. and Yavari, R. (2014c), "Multi-scale computation-based design of nano-segregated polyurea for maximum shockwave-mitigation performance", *AIMS Materials Science*, Vol. 1 No. 1, pp. 15-27.

Grujicic, M., Snipes, J.S., Ramaswami, S., Yavari, R. and Ramasubramanian, M.K. (2014a), "Meso-scale computational investigation of shock-wave attenuation by trailing release-wave in different grades of polyurea", *Journal of Materials Engineering and Performance*, Vol. 23 No. 1, pp. 49-64.

Grujicic, M., Arakere, A., Pandurangan, B., Grujicic, A., Littlestone, A.A. and Barsoum, R.S. (2012a), "Computational investigation of shock-mitigation efficacy of polyurea when used in a combat helmet: a core sample analysis", *Multidiscipline Modeling in Materials and Structures*, Vol. 8 No. 3, pp. 297-331.

Grujicic, M., Bell, W.C., Pandurangan, B., Cheeseman, B.A., Fountzoulas, C. and Patel, P. (2012e), "Molecular-level simulations of shock generation and propagation in soda-lime glass", *Journal of Materials Engineering and Performance*, Vol. 21 No. 8, pp. 1580-1590.

Grujicic, M., d'Entremont, B.P., Pandurangan, B., Runt, J., Tarter, J. and Dillon, G. (2012b), "Concept-level analysis and design of polyurea for enhanced blast-mitigation performance", *Journal of Materials Engineering and Performance*, Vol. 21 No. 10, pp. 2024-2037.

Grujicic, M., He, T., Pandurangan, B., Svingala, F.R., Settles, G.S. and Hargather, M.J. (2011b), "Experimental characterization and material-model development for microphase-segregated polyurea: an overview", *Journal of Materials Engineering and Performance*, Vol. 21 No. 1, pp. 2-16.

Grujicic, M., Pandurangan, B., Bell, W.C., Cheeseman, B.A., Patel, P. and Gazonas, G.A. (2011h), "Molecular-level analysis of shock-wave physics and derivation of the hugoniot relations for soda-lime glass", *Journal of Materials Science*, Vol. 46 No. 22, pp. 7298-7312.

Grujicic, M., Pandurangan, B., Bell, W.C., Cheeseman, B.A., Yen, C.-F. and Randow, C.L. (2011e), "Molecular-level simulations of shock generation and propagation in polyurea", *Materials Science and Engineering A*, Vol. 528 Nos 10/11, pp. 3799-3808.

Grujicic, M., Pandurangan, B., He, T., Cheeseman, B.A., Yen, C.-F. and Randow, C.L. (2010b), "Computational investigation of impact energy absorption capability of polyurea coatings via deformation-induced glass transition", *Materials Science and Engineering A*, Vol. 527 Nos 29/30, pp. 7741-7751.

Grujicic, M., Pandurangan, B., King, A.E., Runt, J., Tarter, J. and Dillon, G. (2011c), "Multi-length scale modeling and analysis of microstructure evolution and mechanical properties in polyurea", *Journal of Materials Science*, Vol. 46 No. 6, pp. 1767-1779.

Grujicic, M., Ramaswami, S., Snipes, J.S., Yavari, R., Yen, C.-F. and Cheeseman, B.A. (2013b), "Axial-compressive behavior, including kink-band formation and propagation, of single p-phenylene terephthalamide (ppta) fibers", *Advances in Materials Science and Engineering*, Vol. 2013, Article ID 329549, pp. 1-15.

Grujicic, M., Snipes, J.S., Ramaswami, S., Galgalikar, R., Runt, J. and Tarter, J. (2013c), "Molecular- and domain-level microstructure dependent material model for nano-segregated polyurea", *Multidiscipline Modeling in Materials and Structures*, Vol. 9 No. 4, pp. 548-578.

Grujicic, A., LaBerge, M., Grujicic, M., Pandurangan, B., Runt, J., Tarter, J. and Dillon, G. (2012g), "Potential improvements in shock-mitigation efficacy of a polyurea-augmented advanced combat helmet: a computational investigation", *Journal of Materials Engineering and Performance*, Vol. 21, pp. 1562-1579.

Grujicic, M., Pandurangan, B., Zhang, Z., Bell, W.C., Gazonas, G.A., Patel, P. and Cheeseman, B.A. (2012f), "Molecular-level analysis of shock-wave physics and derivation of the hugoniot relations for fused silica", *Journal of Materials Engineering and Performance*, Vol. 21 No. 6, pp. 823-836.

Grujicic, M., Snipes, J.S., Ramaswami, S., Yavari, R., Runt, J., Tarter, J. and Dillon, G. (2013a), "Coarse-grained molecular-level analysis of polyurea properties and shock-mitigation potential", *Journal of Materials Engineering and Performance*, Vol. 22 No. 7, pp. 1964-1981.

Grujicic, M., Yavari, R., Snipes, J.S., Ramaswami, S., Runt, J., Tarter, J. and Dillon, G. (2012d), "Molecular-level computational investigation of shock-wave mitigation capability of polyurea", *Journal of Materials Science*, Vol. 47 No. 23, pp. 8197-8215.

Grujicic, M., Bell, W.C., Pandurangan, B., Cheeseman, B.A., Fountzoulas, C., Patel, P., Templeton, D.W. and Bishnoi, K.D. (2011f), "The effect of high-pressure densification on ballistic-penetration resistance of a soda-lime glass", *Journal of Materials: Design and Applications*, Vol. 225 No. 4, pp. 298-315.

Grujicic, M., d'Entremont, B.P., Pandurangan, B., Grujicic, A., LaBerge, M., Runt, J., Tarter, J. and Dillon, G. (2012c), "A study of the blast-induced brain white-matter damage and the associated diffuse axonal injury", *Multidiscipline Modeling in Materials and Structures*, Vol. 8 No. 2, pp. 213-245.

Grujicic, M., Bell, W.C., Glomski, P.S., Pandurangan, B., Cheeseman, B.A., Fountzoulas, C., Patel, P., Templeton, D.W. and Bishnoi, K.D. (2011g), "Multi-length scale modeling of high-pressure induced phase transformations in soda-lime glass", *Journal of Materials Engineering and Performance*, Vol. 20 No. 7, pp. 1144-1156.

IUPAC Gold Book (2013), Bond order, available at: http://goldbook.iupac.org/B00707.html (accessed November 22, 2013).

Kim, H., Citron, J., Youssef, G., Navarro, A. and Gupta, V. (2012), "Dynamic fracture energy of polyurea-bonded steel/E-glass composite joints", *Mechanics of Materials*, Vol. 45 No. 1, pp. 10-19.

Kingery, W.D., Bowen, H.K. and Uhlmann, D.R. (1976), *Introduction to Ceramics*, 2nd ed., John Wiley & Sons, New York, NY, pp. 91-124.

Liu, L., Liu, Y., Zybin, S.V., Sun, H. and Goddard, W.A. (2011), "ReaxFF-lg: correction of the reaxff reactive force field for london dispersion, with applications to the equations of state for energetic materials", *Journal of Physical Chemistry A*, Vol. 115 No. 40, pp. 11016-11022.

Pronin, A.N. and Gupta, V. (1998), "Measurement of thin film interface toughness by using laser-generated stress pulses", *Journal of the Mechanics and Physics of Solids*, Vol. 46 No. 3, pp. 389-410.

van Duin, A.C.T., Dasgupta, S., Lorant, F. and Goddard, W.A. III (2001), "ReaxFF: a reactive force field for hydrocarbons", *Journal of Physical Chemistry A*, Vol. 105 No. 41, pp. 9396-9409.

Wang, X. and Gupta, V. (2006), "Measurement of the intrinsic strength and intrinsic and total fracture resistances of stainless steel/E-glass composite joints," *Journal of Adhesion Science and Technology*, Vol. 20 No. 11, pp. 1171-1188.

Web references

http://accelrys.com/products/datasheets/materials-visualizer.pdf (accessed November 25, 2013).

http://accelrys.com/products/datasheets/amorphous-cell.pdf (accessed November 25, 2013).

http://accelrys.com/products/datasheets/discover.pdf (accessed November 25, 2013).

About the authors

Dr M. Grujicic: Clemson University, Professor, Mechanical Engineering. Research interests include computational engineering. Dr M. Grujicic is the corresponding author and can be contacted at: gmica@clemson.edu

R. Yavari: Clemson University, Graduate Student, Mechanical Engineering. Research interests include multi-physics modeling of various materials phenomena and processes.

Dr J.S. Snipes: Clemson University, Post-Doctoral Fellow, Mechanical Engineering. Research interests include computational material modeling.

Dr S. Ramaswami: Clemson University, Post-Doctoral Fellow, Mechanical Engineering. Research interests include computational material modeling.

Dr R.S. Barsoum: Office of Naval Research, Manager, Explosion Resistant Coating. Research interests include shock propagation studies.